Terahertz Plasmonic Technology

Michael S. Shur, *Life Fellow, IEEE*

***Abstract*—The terahertz (THz) technology has found applications ranging from astronomical science and earth observation to compact radars, non-destructive testing, chemical analysis, explosive detection, moisture content determination, coating thickness control, film uniformity determination, structural integrity testing wireless covert communications, medical applications (including skin cancer detection), imaging, and concealed weapons detection. Beyond 5G Wi-Fi and Internet of Things (IoT) are the expected killer applications of the THz technology. Plasmonic TeraFETs such as Si CMOS with feature sizes down to 3 nm could enable a dramatic expansion of all these applications. At the FET channel sizes below 100 nm, the physics of the electron transport changes from the collision dominated to the ballistic or quasi-ballistic transport. In the ballistic regime, the electron inertia and the waves of the electron density (plasma waves) determine the high frequency response that extends into the THz range of frequencies. The rectification and instabilities of the plasma waves support a new generation of THz and sub-THz plasmonic devices. The plasmonic electronics technology has a potential become a dominant THz electronics sensing technology when the plasmonic THz sources join the compact, efficient, and fast plasmonic TeraFET THz detectors already demonstrated and being commercialized.**

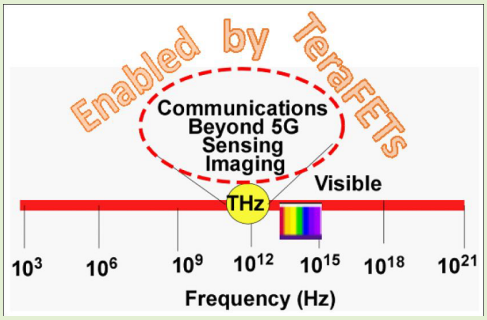

***Index Terms*— Field effect transistors, TeraFETs, plasmonics, terahertz technology, ballistic transport, ballistic mobility.**

I. Introduction

THE terahertz (THz) frequency range (often referred to as the THz gap) lies between the frequency ranges of the electronic and photonic devices. It is the next frontier of ultra-high speed electronics. First applications of the THz technology were in astronomical science [1], [2] and earth observation [3], [4]. In addition to radio astronomy and earth remote sensing, numerous applications of the THz technology include vehicle radars [5] and compact radars [6], [7], non-destructive testing [8], [9], sensing [10]–[12], chemical analysis [13], explosive detection [14], moisture content determination, coating thickness control [15], film uniformity determination [16], structural integrity testing, wireless and wireless covert communications [17]–[22], biotechnology [23]–[30], semiconductor characterization, [31], medical applications [32], [33] (including cancer detection [34], [35]), imaging [36], [37], quantum measurements [38], [39], semiconductor wafer characterization, [40], [41], VLSI testing [42]–[48] concealed weapons detection [49], and food safety control [50], [51]. The expected killer applications are in beyond 5GWi-Fi [52], [53] (with estimated market potential of $730 billion by year 2030 [54]) and Internet of Things (approximately $20 billion market potential in 10 years [55]) using the 230-340 GHz band [19], [20], [56]. The overall THz market has remained modest but is expected to grow from approximately $220 million in 2020 to $1.3 billion in 2027 [57]. However, this growth rate might increase dramatically because of the emerging THz plasmonic technology enabling fast, inexpensive THz detectors, mixers, frequency multipliers, and sources, Focused plane Arrays (FPAs), and THz cameras [58]. This technology is compatible with modern Si VLSI technology and could take advantages of well-developed Si VLSI readout technology used for infrared FPAs and infrared cameras. Figure 1 shows the THz application areas, where the expected impact of the plasmonic THz technology will be the largest.

The paper is organized as follows. Section II considers existing and potential applications of the THz technology that are expected to be impacted by field effect transistors operating in the plasmonic regime (TeraFETs). Section III describes the physics of ballistic and quasi-ballistic transport in short channel TeraFETs and the physics of resonant and overdamped plasma waves. Section IV reviews the state-of-the performance of the THz plasmonic devices. The focus of Section V is

Manuscript received July 30, 2020; revised August 29, 2020; accepted September 5, 2020. Date of publication September 8, 2020; date of current version May 28, 2021. This work was supported in part by the U.S. Air Force Office of Scientific Research under Grant FA9550-19-1-0355 (Project Manager Dr. Ken Goretta), in part by the Army Research Office under Grant W911NF-17-S-0002 (Project Manager Dr. John Qiu), and in part by the Army Research Laboratory under ARL MSME Alliance (Project Manager Dr. Meredith Reed). The associate editor coordinating the review of this article and approving it for publication was Dr. Qammer H. Abbasi.

The author is with the Department of Electrical, Computer, and Systems Engineering, Rensselaer Polytechnic Institute, Troy, NY 12180 USA, and also with Electronics of the Future, Inc., Vienna, VA 22181 USA (e-mail: shurm@rpi.edu).

Digital Object Identifier 10.1109/JSEN.2020.3022809

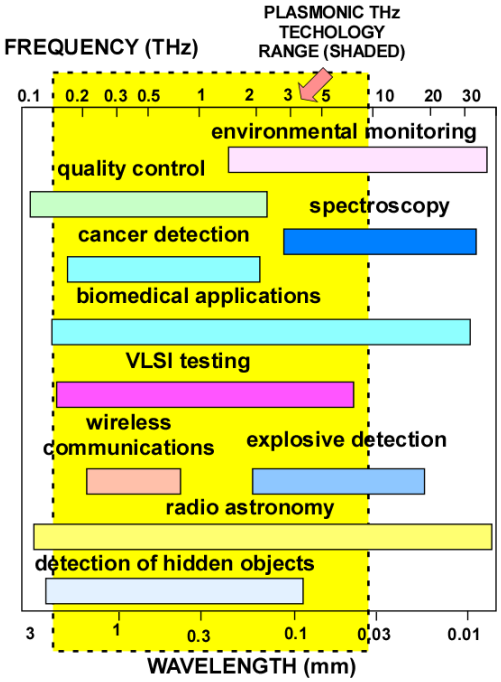

Fig. 1. Subranges of the THz radiation spectrum mapped into different applications. Shaded region show the range, where plasmonics THz technology will have an impact.

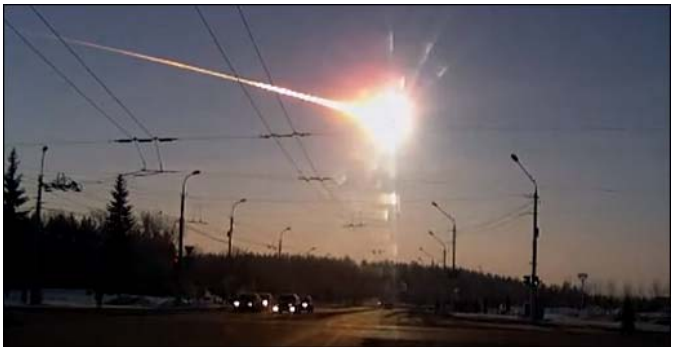

Fig. 2. Chelyabinsk meteorite explosion.

on the new ideas of using plasmonic crystals for detecting, processing, and generating THz radiation.

II. Applications

The Chelyabinsk meteor entered Earth's atmosphere over Russia on 15 February 15, 2013. This undetected near-Earth asteroid travelling with a speed of over 60,000 km/h exploded in an air over the Chelyabinsk region [59] (see Fig. 2). The total kinetic energy of the explosion was over 30 times larger than the energy released by the atomic bomb detonated over Hiroshima. The blast damaged 7,200 buildings and injured 1,500 people. Miraculously, nobody died.

This catastrophic event highlighted the importance of monitoring the space, and THz radiation is an important tool of space exploration. A sub-THz interferometer (IRAM) in Plateau de Bure, French Alps operates at 230 GHz. The of six 15 meters diameter antennas of the IRAM interferometer can move on rail tracks up to a maximum separation of 408 m in the East-West direction and 232 m in the North-South

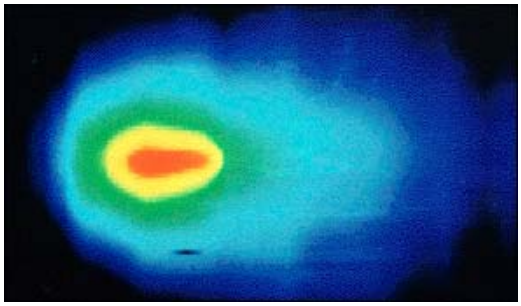

Fig. 3. The image the Iras-Araki-Alcock Comet taken at 12 THz [61].

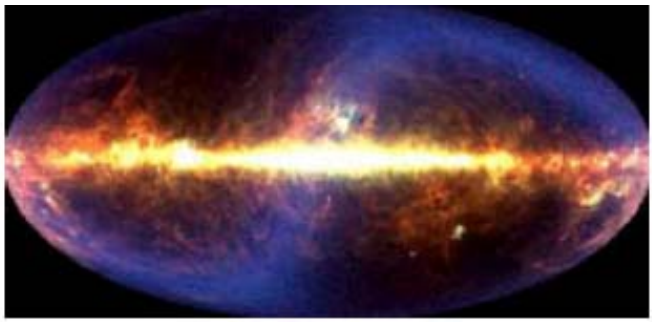

Fig. 4. Stars invisible in a dense dust cloud appear as bright stripe in the THz image [62]. Copyright: Michael Hauser (Space Telescope Science Institute), the COBE/DIRBE Science Team, and NASA.

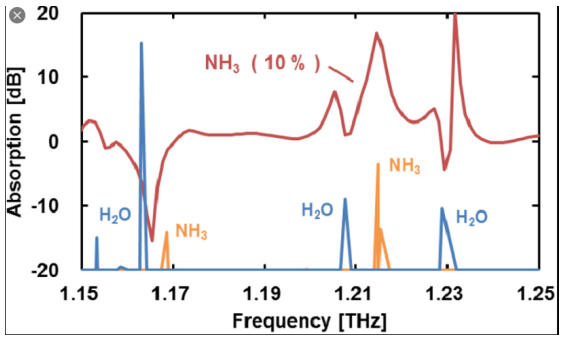

Fig. 5. THz gas spectroscopy [63].

direction. The instrument resolution of 0.5 arcsecs is sufficient to resolving an apple at a distance of 30 km).

COBE, MIRO, ODIN, AKARI, AURA, HERSHEL, IRAS, PLANK, SMILES are examples of THz instruments or missions in space [60]. Fig. 3 shows the image of a comet (called the Iras-Araki-Alcock Comet) was discovered by Infrared Astronomical Satellite (IRAS) in its 560-mile-high, near-polar orbit above the Earth.

Fig. 4 presents another striking example of the THz applications in radio astronomy. THz detects cold matter (140 K or less), such as clouds of gas and dust in our and nearby galaxies. New stars radiate heat are clearly seen in the THz range. Stars invisible in a dense cloud of dust appear as very bright stripe in the THz image because they heat the dust that glows in far-infrared range [62].

THz gas spectroscopy is perfect for detection and identification of gases (see Fig. 5)

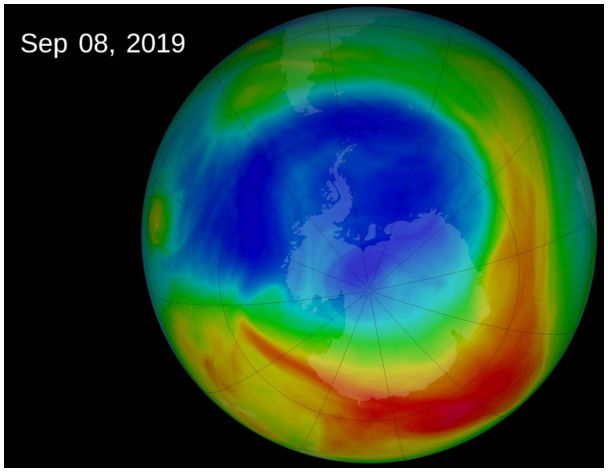

Fig. 6. Ozone hole revealed the NASA study [65].

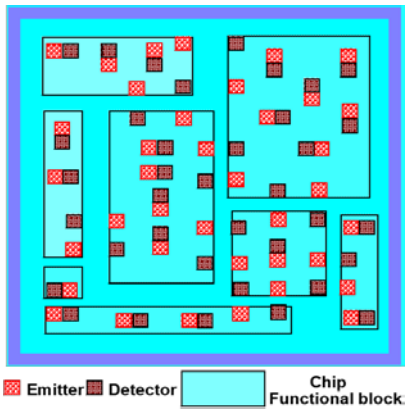

Fig. 7. THz communication on a nanoscale [66].

NASA used the THz spectroscopy for monitoring the ozone and other gases (see Fig. 6). The ozone hole in upper atmosphere lets dangerous ultraviolet radiation pass through causing skin cancer. One out of five Americans will develop skin cancer over their lifetime [64].

THz radiationt penetrates fog and dust, goes through walls, allows for line-of-sight communications with or without reflections, very secure, hard to jam. The communication range varies from light years in space exploration to hundreds of meters in a city environment to the nanoscale for communications inside of a computer board or a computer chip (see Fig. 7). THz communication links are perfect for creating driverless car infrastructure in a large urban environment (see Fig. 8).

Fig. 9 illustrates the increasing demand for the bandwidth by the generations of the cellular networks that could be only addressed by sub-THz (220 GHz to 340 GHz) and THz technologies.

Fig. 10 shows the results of the explosive detection uisng the THz radiation. Fig. 11 shows an example of using sub-THz radiation for identifying toxic gases [67].

Fig. 12 shows the heparin detection by a TeraFET. The sensivity is oreder of magnitude larger that for the ChemFET operation monitoring the changes in the transfer characterisicts when the FET is exposed to heparin.

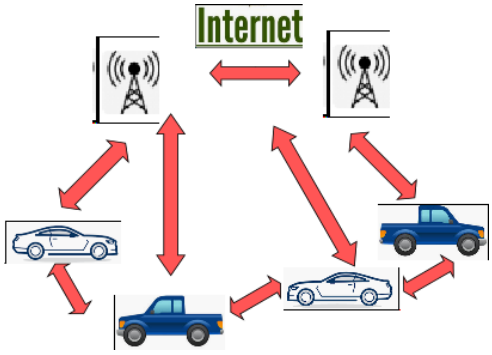

Fig. 8. THz communication links for driverless car infrastructure in a large urban environment.

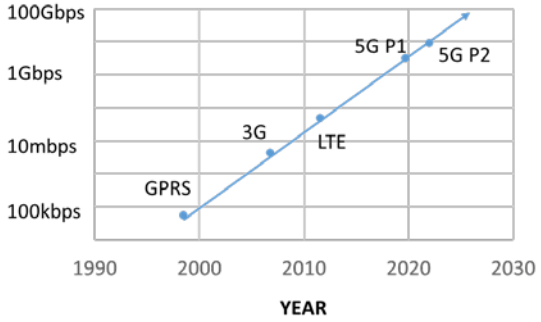

Fig. 9. Increasing demand for the bandwidth by the generations of the cellular networks.

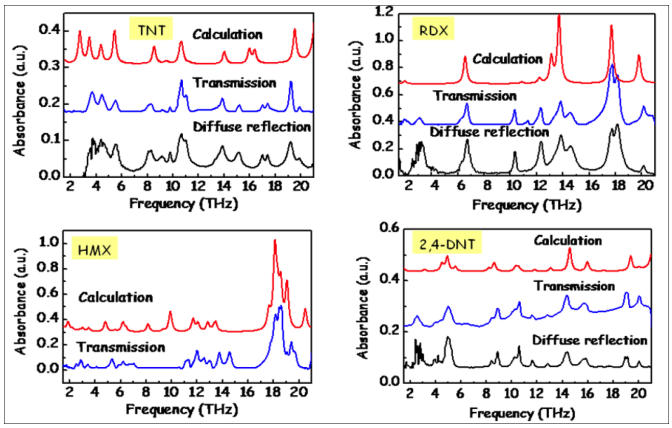

Fig. 10. Diffuse reflection of THz radiation for explosive detection [14].

Fig. 13 present a few more applications that are expected to benefit from the plasmonic TeraFET technology.

Another recently emerging application is in cyber security and defect and reliability studies of short channel field effect transistors (see Fig. 14 and 15). This technique could complement and improve upon more traditional VLSI THz testing (see. Fig. 16 and 17).

III. Physics of TeraFETs: Ballistic Transport and Plasmonics

Fig. 18 shows the power levels achieved by different THz electronic sources [44]. As seen powers generated by Si CMOS and InP-based HEMTs fit well into the overall power

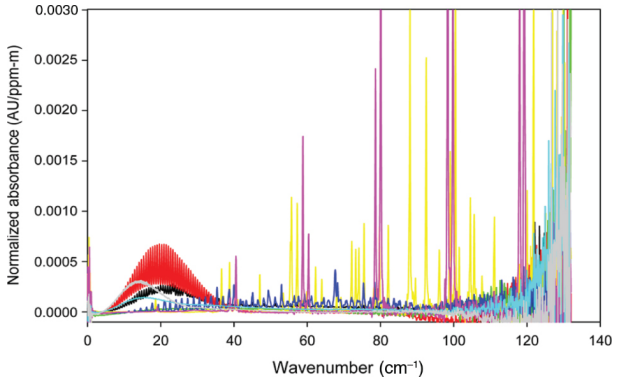

Fig. 11. THz spectra of acetaldehyde (black), acetonitrile (red), ethanol (green), water (yellow), methanol (blue), ammonia (magenta), propionaldehyde, propioaldehyde (cyan), and propanenitrile propionitrile (gray) [67].

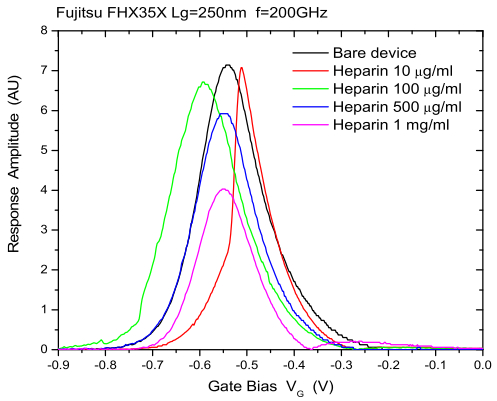

Fig. 12. Transfer characteristics with and without heparin and response of the plasma wave detector [29].

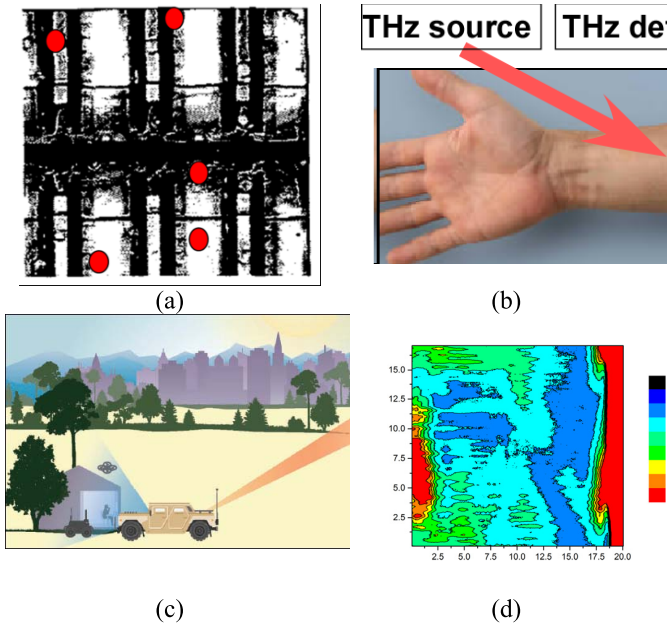

Fig. 13. The results of inspection of space shuttle insulation foam defects using a 0.2 THzGunn diode oscillator (circles indicate the found faults) [9] (a); schematics of THz skin cancer detection (b); THz communication [17] (c); sub-THz image of I7 microprocessor at $f = 288$ GHz [68] (d).

versus frequency dependence. Further improvement of their performance require design optimization based on better understanding of the device physics of ultra-short devices.

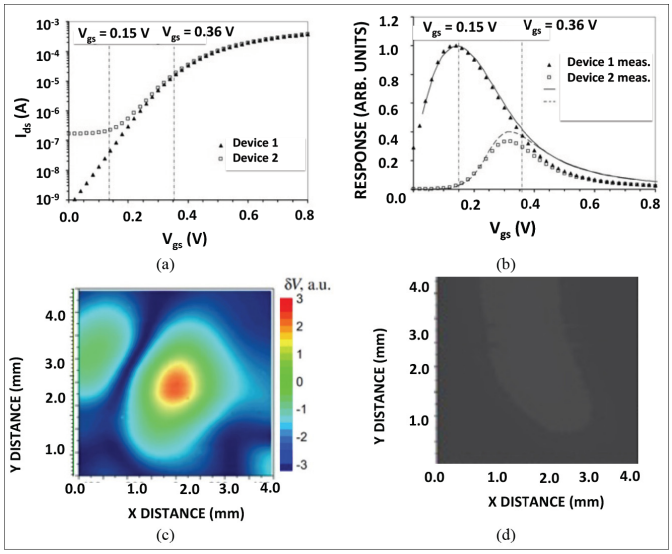

Fig. 14. Measured transfer characteristics (a), 0.2 THz responses (b) of two Si NMOS devices. $L_g = 180$ nm, 0.2 THz response images of normal (c) and defective (d) Si MOS. (After [44]).

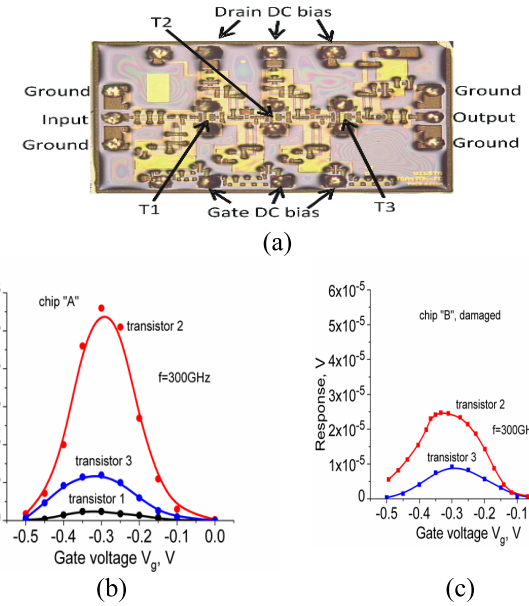

Fig. 15. Testing MMIC under bias by measuring voltage at the package pins: MMIC photograph (a), working device (b) and damaged device (c) responses [47].

Scaling the FET feature sizes below 20 nm required a radically different FIN FET geometry. Further scaling down to 5 nm and 3 nm feature sizes required all around gate design. Such design concepts were first proposed in late 1990's [71]–[73] (see Figures 19 and 20) but it took nearly 20 years for these designs to become mainstream Si MOS VLSI technology.

The physics of the electron transport in such devices involves ballistic and quasi-ballistic transport [74]–[92]. The electron inertia responsible for the excitations of the oscillations of the electron density (the plasma waves) plays a key role in determining the high frequency response.

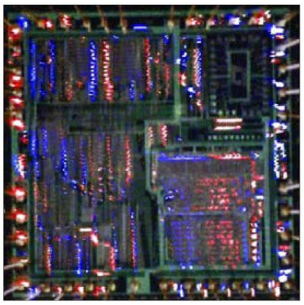

Fig. 16. THz emission image of an LSI microprocessor superimposed on its optical image. From [69].

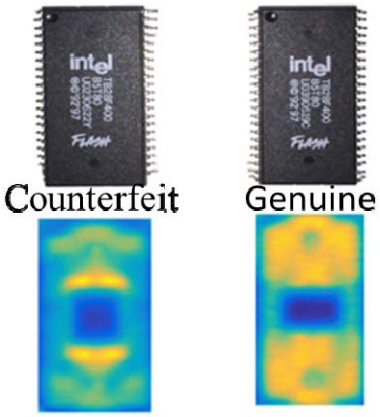

Fig. 17. Optical and THz images of genuine and counterfeit VLSI [48].

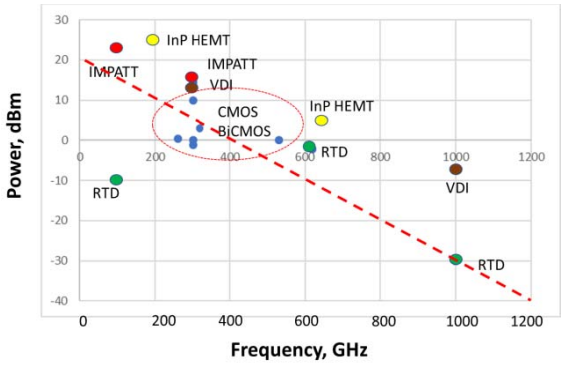

Fig. 18. Power levels of different electronic THz sources [70].

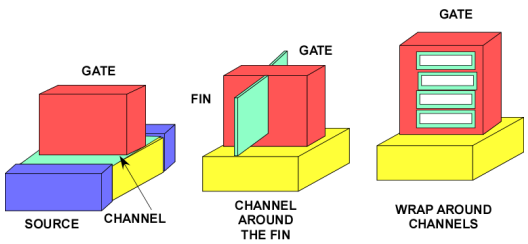

Fig. 19. Conventional, Fin FET and All around Gate designs.

Fig. 21 illustrates ballistic, hydrodynamic ballistic, collision dominated, and hydrodynamic ballistic transport strongly affected by contacts modes of the electron transport in the FET channels.

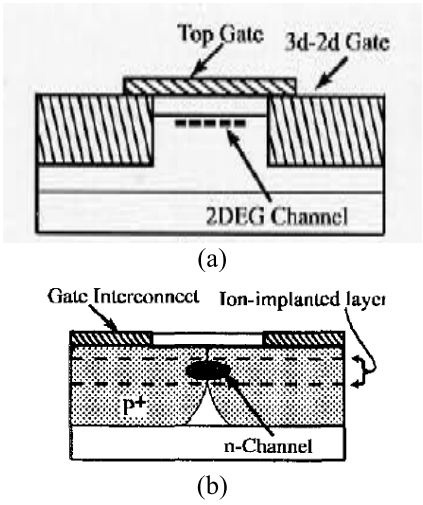

Fig. 20. Heterodimensional HFET designs with the gates on three sides of the channel (like in a FINFET) (a) and coaxial FET (like an all around gate) [71], [72] (b).

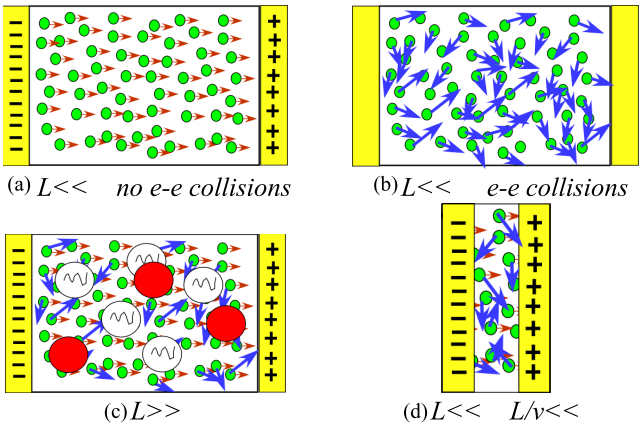

Fig. 21. Electron transport in FET channels: (a) ballistic transport: no electron collisions with impurities and lattice vibrations and no electron-electron collisions; (b) hydrodynamic ballistic transport: no electron collisions with impurities and lattice vibrations and dominant electron-electron collisions; (c) drift-diffusion transport: electron collisions with impurities and lattice vibrations and electron-electron collisions; (d) hydrodynamic ballistic transport strongly affected by contacts. Here v is the largest of the thermal velocity and the Fermi velocity, is the momentum relaxation time.

The characteristic distance determing the modes of the electron transport is the mean free path $\lambda = \upsilon_{th}\tau$ and $\lambda = \upsilon_F\tau$ for a non-degenerate and a degenerate semiconductor, respectively. Here υ_{th} and υ_F are the thermal and Fermi velocity, respectively, and τ is the momentum relaxation time. The ballistic regime takes place when the electron transit length, $L \ll \lambda$.

Fig. 22 showing the evolution of the electron velocity for electrons injected into semiconductor for different values of the electric field illustrates this point. As seen, the electron velocity is higher than the steady-state value reached deep inside the semiconductor. This " overshoot" effect is due to the finite energy relaxation time it takes for the electrons to gain energy from the electric field and, hence, an ability to emit optical phonons. Even more interesting is the electron velocity

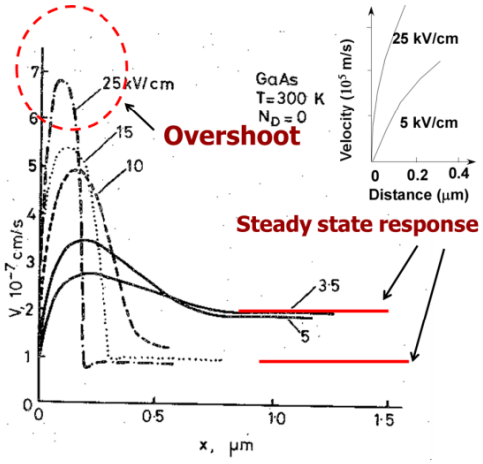

Fig. 22. Evolution of the electron velocity for electrons injected into semiconductor for different values of the electric field [74].

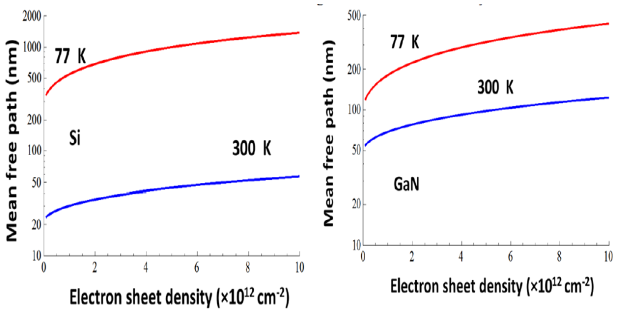

Fig. 23. Mean free path for the two-dimensional electron gas (2DEG) for Si and GaN at 300 K and 77 K.

dependence on distance at very small distances shown in the inset in Fig. 22. At such short distances smaller than the mean free path, the electron transport is not affected by the electron collisions with the impu\rities or lattice vibrations.

Fig. 23 shows typical values of the mean free path for Si and GaN. As seen, the 2DEG mean free path is much larger than the minimum feature size of modern Si CMOS even at room temperature. Therefore, understanding of the physics of the ballistic transport is crucial for the design of modern VLSI.

Fig. 24 illustrates one of the consequences of the hydrodynamic ballistic transport strongly affected by contacts, which the dependence of the apparent (measured) electron mobility on the channel length. As shown in [76], [77] the apparent "ballistic" mobility $\mu_{bal} = \alpha q L/(m\upsilon)$ is determined by the contacts is dominant at short channel length and is proportional to the channel length L : Here m is the electron effective mass, and the constant α and velocity υ are listed in Table I.

The AC impedance of a ballistic device is also dramatically different from that for long channel devices, since that phase relations between the electron fluxes injected form the opposite contacts start playing a dominant role [87].

Hydrodynamic model decribing electrons in TeraFET channels as an electronic fluid provides an insight into the consequencies of the ballistic transport.

Fig. 25 shows the characteristic response time of a semiconductor calculated in the frame of a hydrodynamic model [93].

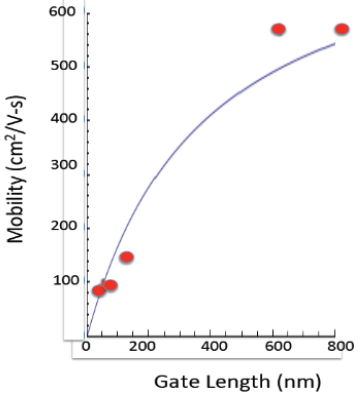

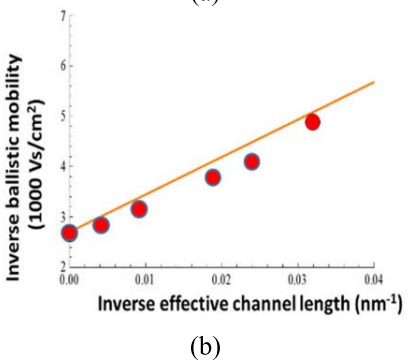

Fig. 24. Ballistic mobility versus channel length for Si. [91] (a) [92] © IEEE2016 (b).

TABLE I
EFFECTIVE VELOCITY $v = v_F$ OR $v = v_{th}$ AND CONSTANT α [AFTER [87]

	Degenerate	Non-degenerate
2D	$\alpha = \frac{2}{\pi};\ v_F = \frac{\hbar\sqrt{2\pi n_s}}{m}$	$\alpha = \frac{1}{2};\ v_{th} = \sqrt{\frac{\pi k_B T}{2m}}$
3D	$\alpha = \frac{3}{4};\ v_F = \frac{\hbar\left(3\pi^2 n\right)^{3/4}}{m}$	$\alpha = \frac{2}{\pi};\ v_{th} = \sqrt{\frac{8k_B T}{\pi m}}$

As seen, at low mobility values (corresponding to the collision-dominated regime) the response time decreases with the electron mobility because it is determined by the electron transit time. However, for high mobilities, when the momentum relaxation time becomes larger than the transit time, the response time increases with the mobility. The reason for this increase is the oscillations of the electron density – plasma waves – that become resonant at high momentum relaxation times, i.e. at high mobility values. For very momentum relaxation times, the electron viscosity becomes a dominant attenuation mechanism and, as seen in Fig. 25, the response time saturates in the viscous electron transport regime.

The saturation level depends on the channel length and on the momentum relaxation time [94]–[96]. The detailed COMSOL simulations of the minimum response time based on the hydrodynamic model are presented in [96] for the 2DEG in InGaAs, Si, GaN, and for the two-dimensional hole gas in p-diamond.

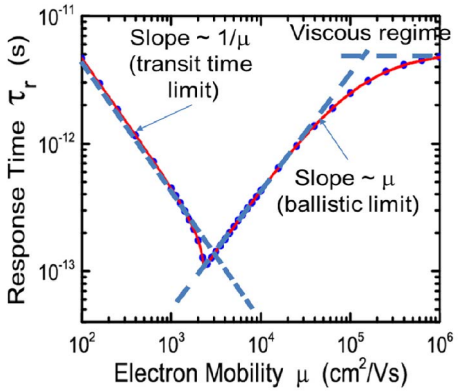

Fig. 25. Characteristic response time of a semiconductor as a function of the electron mobility [94].

The simulation results reported in [96] agree well with analytical theory developed in [94] yielding the characteristic inverse response time $1/\tau_r$ in the frame of the hydrodynamic model

$$\frac{1}{\tau_r} = Re\frac{1}{2}\left[-\left(\frac{1}{\tau}+\frac{\pi^2\nu}{4L^2}\right)+\sqrt{\left(\frac{1}{\tau}+\frac{\pi^2\nu}{4L^2}\right)-\frac{\pi^2 s^2}{L^2}}\right]$$

Here s is the plasma wave velocity given by [97]

$$s = s_o\sqrt{\left[1+\exp\left(-\frac{qV_o}{\eta k_B T}\right)\right]\ln\left[1+\exp\left(\frac{qV_o}{\eta k_B T}\right)\right]}$$

V_o is the gate voltage swing ($V_o = V_G - V_T$ with V_G and V_T being the gate and threshold voltage, respectively), T is temperature, $s_o = \sqrt{\eta k_B T/m}$, η is the subthreshold ideality factor, T is temperature, k_B is the Boltzmann constant. The typical values of the plasma velocity are much larger that the electron drift velocity and the values of the fundamental plasma frequency correspond to the THz range (see Fig. 25). The fundamental frequency of the plasma waves for electrons in a gated MOS channel biased above threshold is $f_{pa} = s/(4L)$ and $f_{ps} = s/(2L)$ for asymmetric and symmetric boundary conditions, respectively.

As seen from Fig. 26, the plasma wave velocity is much larger than the electron drift velocity in long channel devices, and a typical fundamental plasma frequency is much large than the FET cutoff frequency, which is on the order of the inverse transit time.

Fig. 27 (from [98]) shows the dispersion relations for the plasma waves in different TeraFET regions.

As seen from Fig. 26, the plasma wave velocity and the fundamental plasma frequency could vary from 2×10^5 m/s to over 10^6 m/s and from 0.2 THz to 10 THz, respectively. Hence, the plasmonic TeraFETs could cover most of the THz range (0.3 THz to 30 THz). Plasma wave excitation in submicron FET and related device structures could support a new generation of solid-state terahertz tunable devices discussed in the next section.

The phenomena described in this Section could be affected by contacts, surface scattering, and impedance mismatch.

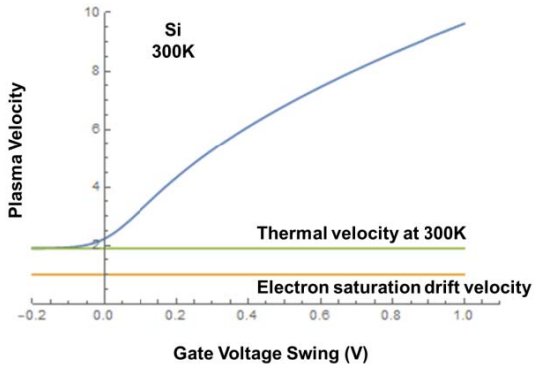

Fig. 26. Comparison of plasma, drift, and thermal velocities for Si FETs. (From [98]).

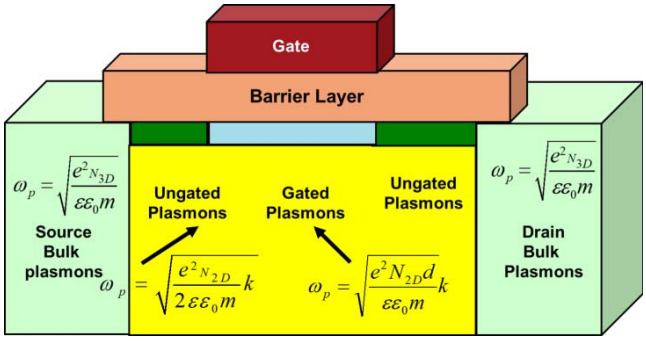

Fig. 27. Dispersion relations for plasma waves. N_{2D} and N_{3d} are sheet and bulk carrier concentrations, k is the wave vector. (From [98]).

The compact models [99] and TCAD simulations [92] are very useful in evaluating the contribution of these non-ideal effects.

IV. THz Plasmonic Devices

The first proposal to use the plasma instability in a ballistic or quasi-ballistic TeraFET channel for generating THz radiation [100] relied on the different plasma wave reflections from the channel boundaries with the channel serving as a resonant cavity for the plasma waves. This instability now (called the Dyakonov-Shur instability) predicts a relatively narrow THz emission spectrum. The Ryzhii-Satou-Shur transit time plasmonic instability [101] involving the transit time delay shifting the phase between the THz voltage and current should result in the narrow band THz emission as well. However, most papers reported on the broadband THz radiation emitted from TeraFETs [102]–[109]. A strong and narrow band emission from a single GaAs TeraFET was reported in [110]. The power level was the highest reported for the TeraFETs (63 mW at 300 and 278 mW at 77 K with 0.0486% conversion efficiency) [110]. Further studies are required to understand the mechanism responsible for this emission. Obtaining still higher power levels and higher conversion efficiencies might require collecting radiation from larger areas than just a single short channel TeraFET (see the next Section).

The rectification of the resonant or overdamped plasma oscillations could be used for the detection of the THz radiation [111], [112]. Fig. 28 (from [113]) shows the schematics of a TeraFET THz detectors with a THz signal coupled to the

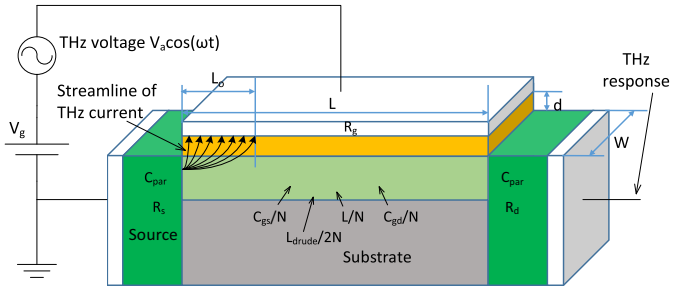

Fig. 28. Plasmonic FET under THz radiation modeled with multiple segments in the channel accounting for the THz current distribution. (From [113] © IEEE2020.

TABLE II
THE VALUES OF Q_m AND f_m FOR SI, GAN, INGAAS, AND p-DIAMOND TERAFETS AT 300 AND 77 K. THE GATE SWING IS CHOSEN TO MAXIMIZE THE QUALITY FACTOR. (FROM [115])

	22 nm		65 nm		130 nm	
	Q_m	f_p	Q_m	f_p	Q_m	f_p
Si (300 K)	7	12	3.5	3.6	1.75	1.8
Si (77 K)	27	3.5	15.2	2	11	1.65
GaN (300 K)	11	10	5.2	3.4	2.7	1.7
GaN (77 K)	47	2.5	28	1.5	18	1
InGaAs (300 K)	8	5	3.5	3	2.8	1.8
InGaAs (77 K)	18	2	7	1	4.5	0.8
p-diamond (300 K)	70	6	25	2	11	1
p-diamond (77 K)	180	3	100	1.5	80	1

TeraFET via the source contact and inducing the oscillations of the electron density in the channel. The figure shows the characteristic distance of the oscillations spatial decay [97]: $L_o = \left(\mu V_{gte}/(2\pi f)\right)^{0.5}$. Here V_{gte} is the effective gate voltage swing [114]. The response depends on the relationship between L and L_o and on the quality factor $Q_m = \omega_p \tau$, where $\omega_p = 2\pi f_p$, f_p is the fundamental plasma frequency, and τ is the momentum relaxation time.

The THz voltage source in Fig. 28 represents the THz signal coupled to the TeraFET via the source contact. Also shown is the equivalent circuit of the TeraFET channel subdivided into many nonlinear transmission line segments to account for the nonuniform distribution of the electron density along the channel. This approach allows for the accurate compact modeling of TeraFETs using ADS or SPICE [99], [113].

Table II (from [115]) shows the estimated values of Q_m and f_p for Si, GaN, InGaAs, and p-diamond TeraFETs at 300 and 77 K. The gate swing was chosen to maximize the quality factor. As seen, a resonant detection ($Q_m \gg 1$) is possible even at room temperature even though non-resonant detection is much easier to achieve.

Fig. 29 (from [116]) shows a typical non-resonant response of Si TeraFET.

Fig. 30 (from [117] shows the Si FINFET response up to approximately 5 THz. A large responsivity drop with an

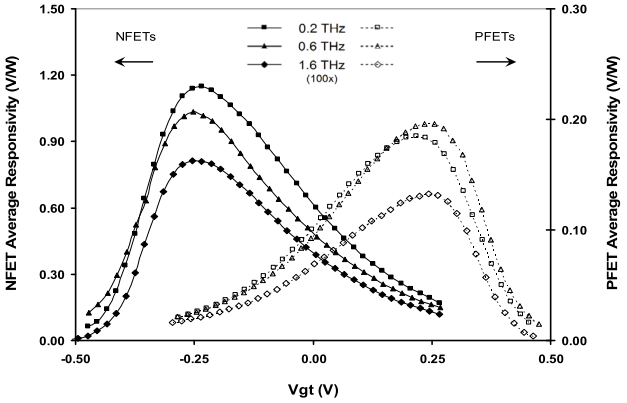

Fig. 29. Sub-THz detection by Si CMOS (from [116]). © IEEE 2007.

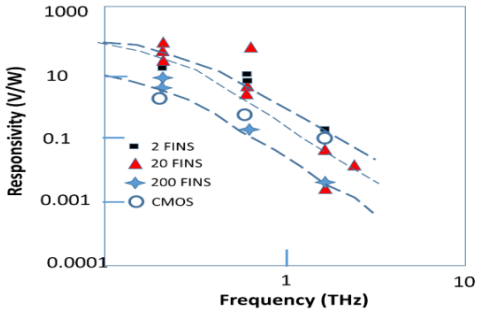

Fig. 30. Plasmonic detectors work up to 5 THz (from [117]).

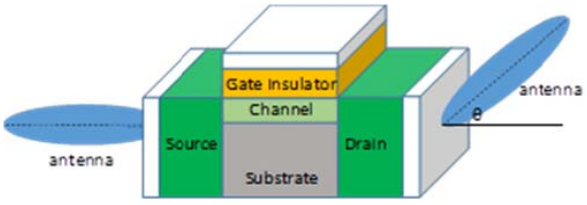

Fig. 31. TeraFET with two antennas [120].

increasing frequency is due to the effect of contacts, parasitics, and skin effect.

As seen from the Table II, Si TeraFETs might become primary candidates for THz components and p-diamond has superb properties for THz applications, especially at the lower frequencies of the THz band [118]. Graphene TeraFETs are also emerging as competitive plasmonic THz detectors [119].

The THz radiation could couple to the both sides of the TeraFET channel (see Fig. 31). The phase difference between the plasma waves excited at the source and drain depends on the plasma frequency and, hence, could be adjusted by the gate bias [113], [120], [121].

An important application of this effect is a vector detection (detecting both the amplitude and the phase of a signal) to be used for a line-of-sight detection. Measuring the gate bias, at which the response becomes equal to zero, allows using TeraFET as a THz spectrometer of interferometer. Fig. 32 shows the simulated frequency ranges, in which TeraFETs could operate as spectrometers.

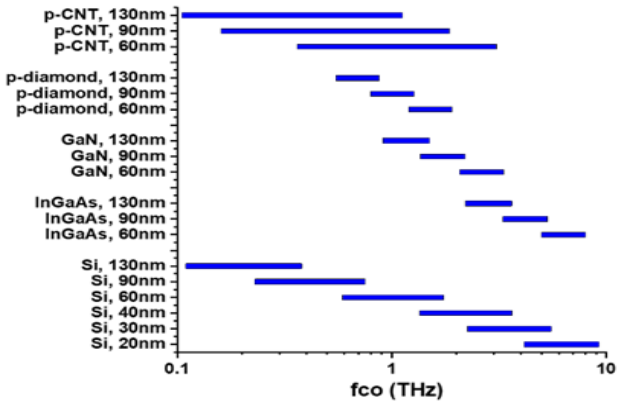

Fig. 32. Cross-over frequency ranges for TeraFETs implemented in different materials [121].

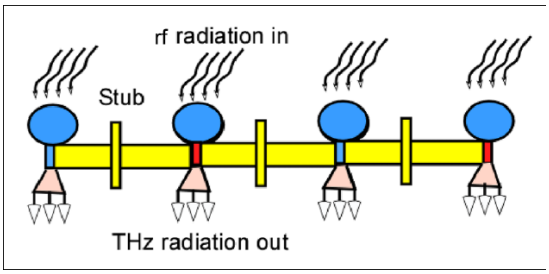

Fig. 33. Stub-split cavity RF-to-THz plasmonic converter crystal [147].

At lower frequencies, plasmonic THz detection becomes inefficient and the dominant detection mechanism becomes a resistive mixing, see [122] for more details.

V. Plasmonic Crystals as Potential THz Radiation Sources and Detectors

The attempts to increase the responsivity involve using the ratchet effect [123]–[128], grated gate structures [129]–[133], plasmonic boom [134], [135], and variable width devices [115]. We call such structures plasmonic crystals with the unit cells smaller or comparable to the mean free path but capable of capturing and processing a larger THz flux.

FET arrays and grating structures already demonstrated superior performance as THz detectors [136]–[141] in a good agreement with theoretical predictions [142]–[145]. Both the Dyakonov-Shur instability [100], [146] and "plasmonic boom" instability [134], [135] can develop in the plasmonic crystals. The plasmonic boom instability develops in a plasmonic crystal with two regions per unit cell with plasma wave velocities in these cells s_1 and s_2, such that $s_1 < \mathrm{v} < s_2$, where v is the velocity of electron flow. This coulbe achieved using different theshold voltages in the cells 1 and 2 or by the cells having a different width. Narrow protruding regions (plasmonic stubs) could adjust the boundary conditions between the sections and the plasmonic crystal with stubs could support RF to THz conversion (see Fig. 33).

VI. Conclusion

Small sizes (making it easy to fabricate arrays), high sensitivity, broad spectral range, band selectivity and tuneability fast temporal response and the compatibility of Si plasmonic TeraFETs with VLSI technology make plasmonic THz technology to be a prime candidate for closing the famous THz gap in the electromagnetic spectrum applications. THz sensing, imaging, and communications are the prime candidates for the application of the THz plasmonics with a strong commercial appeal for deploying Si based 240 GHz to 300 GHz technology for beyond 5G WI FI and IoT applications. Recently reported high narrow-band THz power emitted by a single GaAs-based TeraFET [110] is a breakthrough highlighting the emerging commercial potential of the THz plasmonic technology.

References

[1] P. De Maagt, P. H. Bolivar, and C. Mann, "Terahertz science, engineering and systems—from space to earth applications," *Encyclopedia RF Microw. Eng.*, Apr. 2005, doi: 10.1002/0471654507.eme518.
[2] P. H. Siegel, "THz for space: The golden age," in *IEEE MTT-S Int. Microw. Symp. Dig.*, May 2010, pp. 816–819, doi: 10.1109/MWSYM.2010.5515761.
[3] J. W. Waters, "Submillimeter-wavelength heterodyne spectroscopy and remote sensing of the upper atmosphere," *Proc. IEEE*, vol. 80, no. 11, pp. 1679–1701, Oct. 1992.
[4] B. G. Xia, D. H. Zhang, J. Meng, J. Huang, C. F. Yao, and J. S. Zhang, "Terahertz FSS for space borne passive remote sensing application," *Electron. Lett.*, vol. 49, no. 22, pp. 1398–1399, Oct. 2013, doi: 10.1049/el.2013.2407.
[5] S. Mumtaz, J. Miquel Jornet, J. Aulin, W. H. Gerstacker, X. Dong, and B. Ai, "Terahertz communication for vehicular networks," *IEEE Trans. Veh. Technol.*, vol. 66, no. 7, pp. 5617–5625, Jul. 2017.
[6] A. Ruengwaree, A. Ghose, J. Weide, and G. Kompa, "Ultra-fast pulse transmitter for UWB microwave radar," in *Proc. Eur. Radar Conf.*, Sep. 2006, pp. 354–357.
[7] C. Nguyen and J. Han, "Time-domain ultra-wideband radar," in *Sensor and Components: Theory, Analysis and Design*. Berlin, Germany: Springer-Verlag, 2014, pp. 27–33.
[8] E. Lee *et al.*, "Terahertz non-destructive testing technology for industrial applications," *Electron. Telecommun. Trends*, vol. 33, no. 3, pp. 59–69, 2018.
[9] H. Zhong *et al.*, "Spection of space shuttle insulation foam defects using a 0.2 THz gunn diode oscillator," in *Proc. 12th Int. Conf. Terahertz Electron.*, 2004, pp. 753–754.
[10] M. J. Fitch and R. Osiander, "Terahertz waves for communications and sensing," *Johns Hopkins APL Tech. Dig.*, vol. 25, no. 4, pp. 348–355, 2004.
[11] M. Shur, "Terahertz electronics for sensing applications," in *Proc. IEEE SENSORS*, Oct. 2011, pp. 40–43.
[12] N. Pala and M. Shur, "Devices for sensing, imaging and communication applications," *Proc. SPIE*, vol. 10982, May 2019, Art. no. 109822Y.
[13] T. Kiwa *et al.*, "Imaging of chemical reactions using a terahertz chemical microscope," *Photonics*, vol. 6, no. 1, p. 10, Jan. 2019, doi: 10.3390/photonics6010010.
[14] Y. Chen *et al.*, "THz diffuse reflectance spectra of selected explosives and related compounds," *Proc. SPIE*, vol. 5790, pp. 19–24, May 2005.
[15] M. Shur, "Terahertz electronics for sensing and imaging applications," *Proc. SPIE*, vol. 9467, May 2015, Art. no. 94672A, doi: 10.1117/12.2085442.
[16] S. Krimi, J. Klier, J. Jonuscheit, G. von Freymann, R. Urbansky, and R. Beigang, "Highly accurate thickness measurement of multi-layered automotive paints using terahertz technology," *Appl. Phys. Lett.*, vol. 109, 2016, Article no. 021105.
[17] M. Shur, S. Rudin, G. Rupper, F. Dagefu, and M. Brodsky, "TeraFETs for terahertz communications," *Photon. Newslett.*, vol. 33, no. 3, pp. 4–7, Jun. 2019.
[18] M. Tonouchi, "Cutting-edge terahertz technology," *Nature Photon.*, vol. 1, pp. 97–105, Oct. 2007.
[19] C. Jastrow, K. Munter, R. Piesiewicz, T. Kurner, M. Koch, and T. Kleine-Ostmann, "300 GHz transmission system," *Electron Lett*, vol. 44, pp. 213–214, Feb. 2008.
[20] H.-J. Song *et al.*, "8 Gbit/s wireless data transmission at 250 GHz," *Electron. Lett.*, vol. 45, no. 22, pp. 1121–1122, Oct. 2009.
[21] M. Shur, "Plasmonic detectors and sources for THz communication and sensing," *Proc. SPIE*, vol. 10639, Aug. 2018, Art. no. 1063929.

[22] T. Kleine-Ostmann and T. Nagatsuma, "A review on terahertz communications research," *J. Infr., Millim., THz Waves*, vol. 32, no. 2, pp. 143–171, Feb. 2011.

[23] Q. Sun, Y. He, K. Liu, S. Fan, P. J. Edward Parrott, and E. Pickwell-MacPherson, "Recent advances in terahertz technology for biomedical applications," *Quant. Imag. Med. Surgery*, vol. 7, no. 3, p. 345, 2017.

[24] Y. Hwang *et al.*, "*In vivo* analysis of THz wave irradiation induced acute inflammatory response in skin by laser-scanning confocal microscopy," *Opt. Express*, vol. 22, no. 10, pp. 11465–11475, 2014.

[25] B. S. Alexandrov, V. Gelev, A. R. Bishop, A. Usheva, and K. Ø. Rasmussen, "DNA breathing dynamics in the presence of a terahertz field," *Phys. Lett. A*, vol. 374, no. 10, pp. 1214–1217, Feb. 2010, doi: 10.1016/j.physleta.2009.12.077.

[26] D. F. Plusquellic and E. J. Heilweil, "Terahertz spectroscopy of biomolecules," in *Terahertz Spectroscopy*. Boca Raton, FL, USA: CRC Press, 2007, pp. 293–322.

[27] A. N. Bogomazova *et al.*, "No DNA damage response and negligible genome-wide transcriptional changes in human embryonic stem cells exposed to terahertz radiation," *Sci. Rep.*, vol. 5, no. 1, Jul. 2015, Art. no. 7749.

[28] M. Shur, "Subterahertz and terahertz sensing of biological objects and chemical agents," *Proc. SPIE*, vol. 10531, Feb. 2018, Art. no. 1053108, doi: 10.1117/12.2288855.

[29] N. Pala and M. Shur, "Plasmonic THz detectors for biodetection," *Electron. Lett*, vol. 44, no. 24, p. 1391, 2008.

[30] E. Pickwell and V. Wallace, "Biomedical applications of terahertz technology," *J. Phys. D, Appl. Phys.*, vol. 39, no. 17, p. R301, 2006.

[31] V. Jelic *et al.*, "Ultrafast terahertz control of extreme tunnel currents through single atoms on a silicon surface," *Nature Phys.*, vol. 13, no. 6, pp. 591–598, Jun. 2017.

[32] P. H. Siegel, "Terahertz technology in biology and medicine," *IEEE Trans. Microw. Theory Techn.*, vol. 52, no. 10, pp. 2438–2447, Oct. 2004, doi: 10.1109/TMTT.2004.835916.

[33] H. Hintzsche, C. Jastrow, T. Kleine-Ostmann, U. Kärst, T. Schrader, and H. Stopper, "Terahertz electromagnetic fields (0.106 THz) do not induce manifest genomic damage *in vitro*," *PLoS ONE*, vol. 7, no. 9, Sep. 2012, Art. no. e46397.

[34] C. Yu, S. Fan, and Y. Sun, "Emma pickwell-macPherson, The potential of terahertz imaging for cancer diagnosis: A review of investigations to date," *Quant Imag. Med. Surg.*, vol. 2, no. 1, pp. 33–45, Mar. 2012, doi: 10.3978/j.issn.2223-4292.2012.01.04.

[35] A. Rossi *et al.*, "Mechanisms and immunogenicity of nsPEF-induced cell death in B16F10 melanoma tumors," *Sci. Rep.*, vol. 9, no. 1, Dec. 2019, Art. no. 431.

[36] J.-S. Rieh, D. Yoon, and J. Yun, "An overview of solid-state electronic sources and detectors for terahertz imaging," in *Proc. 12th IEEE Int. Conf. Solid-State Integr. Circuit Technol.*, 2014, pp. 1–4.

[37] R. M. Shur and N. Pala, "Terahertz plasmonic field effect transistors for imaging applications," *Proc. SPIE*, vol. 10982, May 2019, Art. no. 109822Z, doi: 10.1117/12.2517428.

[38] J. Kröll, "Phase-resolved measurements of stimulated emission in a laser," *Nature*, vol. 449, pp. 698–701, May 2007.

[39] I.-C. Benea-Chelmus, F. F. Settembrini, G. Scalari, and J. Faist, "Electric field correlation measurements on the electromagnetic vacuum state," *Nature*, vol. 568, pp. 202–206, Jul. 2019.

[40] D. M. Mittleman, J. Cunningham, M. C. Nuss, and M. Geva, "Noncontact semiconductor wafer characterization with the terahertz Hall effect," *Appl. Phys. Lett.*, vol. 71, no. 1, pp. 16–18, Jul. 1997, doi: 10.1063/1.119456.

[41] M. Farooq and M. Shur, "Inspection system and method for detecting defects at a materials interface," U.S. Patent 10 215 695 Bl, Feb. 26, 2019.

[42] M. Shur, S. Rudin, G. Rupper, M. Reed, and J. Suarez, "Sub-terahertz testing of millimeter wave monolithic and very large scale integrated circuits," *Solid State Electron.*, vol. 155, pp. 44–48, May 2019, doi: 10.1016/j.sse.2019.03.007.

[43] N. Akter, M. Karabiyik, M. Shur, and N. Pala, "AI powered THz testing technology for ensuring hardware cybersecurity," in *Proc. IEEE RAPID Conf.*, Aug. 2020, pp. 1–2.

[44] W. Stillman, D. Veksler, T. A. Elkhatib, K. Salama, F. Guarin, and M. S. Shur, "Sub-terahertz testing of silicon MOSFET," *Electron. Lett.*, vol. 44, no. 22, pp. 1325–1327, Oct. 2008.

[45] N. Akter, M. Karabiyik, M. Shur, J. Suarez, and N. Pala, "AI powered THz VLSI testing technology," in *Proc. NATW*, 2020, pp. 1–5.

[46] M. S. Shur and J. Suarez, "Nanoscale silicon MOSFET response to THz radiation for testing VLSI," in *Proc. IEEE 27th North Atlantic Test Workshop (NATW)*, 2018, p. 1.

[47] S. Rumyantsev *et al.*, "Terahertz beam testing of millimeter wave monolithic integrated circuits," *IEEE Sensors J.*, vol. 17, no. 1, pp. 5487–5490, Sep. 2017.

[48] K. Ahi, S. Shahbazmohamadi, and N. Asadizanjani, "Quality control and authentication of packaged integrated circuits using enhanced-spatial-resolution terahertz time-domain spectroscopy and imaging," *Opt. Lasers Eng.*, vol. 104, pp. 274–284, May 2018.

[49] F. Federici *et al.*, "THz imaging and sensing for security applications-explosives, weapons and drugs," *Semicond. Sci. Technol.*, vol. 20, no. 7, p. S266, 2005.

[50] L. Afsah-Hejri, P. Hajeb, P. Ara, and R. J. Ehsani, "A comprehensive review on food applications of terahertz spectroscopy and imaging," *Comprehensive Rev. Food Sci. Food Saf.*, vol. 18, no. 5, pp. 1563–1621, Sep. 2019.

[51] G. Ok, K. Park, H. S. Chun, H. J. Chang, N. Lee, and S. W. Choi, "High performance sub-terahertz transmission imaging system for food inspection," *Biomed. Opt. Express*, vol. 6, no. 5, pp. 1929–1941, May 2015, doi: 10.1364/BOE.6.001929.

[52] P. T. Dat, A. Kanno, N. Yamamoto, and T. Kawanishi, "Seamless convergence of fiber and wireless systems for 5G and beyond networks," *J. Lightw. Technol.*, vol. 37, no. 2, pp. 592–605, Jan. 15, 2019.

[53] P. Pirinen, "A brief overview of 5G research activities," in *Proc. 1st Int. Conf. 5G Ubiquitous Connectivity (5GU)*, Nov. 2014, pp. 17–22, doi: 10.4108/icst.5gu.2014.258061.

[54] *5G Technology, Market and Forecasts 2020–2030*. Accessed: Jan. 10, 2020. [Online]. Available: https://www.idtechex.com/en/research-report/5g-technology-market-and-forecasts-2020-2030/753

[55] *Internet of Things (IoT) 2017–2027*. Accessed: Jan. 10, 2020. [Online]. Available: https://www.idtechex.com/en/research-report/internet-of-things-iot-2017-2027/499

[56] S. Koenig *et al.*, "Wireless sub-THz communication system with high data rate," *Nature Photon.*, vol. 7, no. 12, pp. 977–981, Dec. 2013.

[57] *Terahertz Technology—Global Market Trajectory & Analytics*, Global Industry Analysts, San Jose, CA, USA, Jul. 2020.

[58] M. Shur (Keynote), "Terahertz nanoplasmonics technology: Physics, applications, and commercialization," *ECS Trans.*, vol. 97, no. 7, p. 369, 2020.

[59] O. P. Popova *et al.*, "Chelyabinsk airburst, damage assessment, meteorite recovery and characterization," *Science*, Nov. 2013, Art. no. 1242642, doi: 10.1126/science.1242642.

[60] P. H. Siegel, "THz instruments for space," *IEEE Trans. Antennas Propag.*, vol. 55, no. 11, pp. 2957–2965, Nov. 2007.

[61] *Comet IRAS-Araki-Alcock*. Accessed: Jan. 10, 2020. [Online]. Available: https://old.ipac.caltech.edu/outreach/Gallery/IRAS/comet.html

[62] *Traces of the Disc Surrounding Our Solar System Are Visible in This Image Taken by Cobe*. Accessed: Jan. 10, 2020. [Online]. Available: https://sci.esa.int/web/home/-/29478-traces-of-the-disc-surrounding-our-solar-system-are-visible-in-this-image-taken-by-cobe

[63] T. Suzuki, T. Katagiri, and Y. Matsuura, "Terahertz gas sensing based on time-domain-spectroscopy using a hollow-optical fiber gas cell," *Proc. SPIE*, vol. 10488, Feb. 2018, Art. no. 1048808, doi: 10.1117/12.2288102.

[64] R. S. Stern, "Prevalence of a history of skin cancer in 2007: Results of an incidence-based model," *Arch Dermatol.*, vol. 146, no. 3, pp. 279–282, Mar. 2010.

[65] *2019 Ozone Hole is the Smallest on Record Since Its Discovery*. Accessed: Jan. 10, 2020. [Online]. Available: https://www.nasa.gov/feature/goddard/2019/2019-ozone-hole-is-the-smallest-on-record-since-its-discovery

[66] Y. Deng and M. S. Shur, "Electron mobility and terahertz detection using silicon MOSFETs," *Solid-State Electron.*, vol. 47, no. 9, pp. 1559–1563, Sep. 2003.

[67] L. Yang, T. Guo, X. Zhang, S. Cao and X. Ding, "Toxic chemical compound detection by terahertz spectroscopy: A review," *Rev. Anal. Chem.*, vol. 37, no. 3, p. 58, Jun. 2018.

[68] M. Shur, "Plasmonic heterodimensional resonance for subwavelength imaging," *Proc. SPIE*, vol. 10639, May 2018, Art. no. 1063907, doi: 10.1117/12.230134.

[69] K. Kawase, "Terahertz imaging for drug detection & large-scale integrated circuit inspection," *Opt. Photon. News*, vol. 15, no. 10, pp. 34–39, Oct. 2004.

[70] M. Shur, "Silicon and silicon germanium terahertz electronics," in *IEEE MTT-S Int. Microw. Symp. Dig.*, Ann Arbor, MI, USA, Jul. 2018, pp. 1–3.

[71] B. Iniguez, J.-Q. Lu, and M. S. Shur, "3D-FET: A new heterodimensional device for high-speed ultra-low power applications," in *Proc. Int. Device Res. Symp. (ISDRS)*, vol. 9, 1999, pp. 61–64.

[72] J.-Q. Lu, M. J. Hurt, W. C. B. Peatman, and M. S. Shur, "Heterodimensional field effect transistors for ultra low power applications," in *Proc. 20th Annual. Tech. Dig.*, 1982, pp. 187–190.

[73] X. Huang, "Sub 50-nm FinFET: PMOS," in *IEDM Tech. Dig.*, Dec. 1999, p. 67.

[74] M. S. Shur, "Influence of non-uniform field distribution in the channel on the frequency performance of GaAs FETs," *Electron. Lett.*, vol. 12, no. 23, pp. 615–616, 1976.

[75] M. S. Shur and L. F. Eastman, "Ballistic transport in semiconductors at low-temperatures for low power high speed logic," *IEEE Trans. Electron Devices*, vol. ED-26, no. 11, pp. 1677–1683, Nov. 1979.

[76] A. A. Kastalsky and M. S. Shur, "Conductance of small semiconductor devices," *Solid State Commun.*, vol. 39, no. 6, pp. 715–718, Aug. 1981.

[77] A. A. Kastalsky, M. S. Shur, and K. Lee, "Conductance of small semiconductor devices," in *Proc. IEEE Cornell Microw. Conf.*, Ithaca, NY, USA, Aug. 1981, pp. 107–114.

[78] M. S. Shur, "Ballistic transport in semiconductor with collisions," *IEEE Trans. Electron. Devices*, vol. ED-28, no. 10, pp. 1120–1130, Oct. 1981.

[79] M. S. Shur and L. F. Eastman, "Near-ballistic transport in GaAs devices at 77 K," *Solid State Electron.*, vol. 24, no. 1, pp. 11–18, Jan. 1981.

[80] L. F. Eastman *et al.*, "Ballistic electron transport in thin layers of GaAs," in *Proc. 8th Int. Symp. Gallium Arsenide Rel. Compounds*, 1981, pp. 185–192.

[81] I. Z. Ren, R. Venugopal, S. Datta, M. S. Lundstrom, D. Jovanovic, and J. G. Fossum, "The ballistic nanotransistor: A simulation study," *IEDM Tech. Dig.*, Dec. 2000, pp. 715–718.

[82] M. S. Shur, "Low ballistic mobility in submicron HEMTs," *IEEE Electron Device Lett.*, vol. 23, no. 9, pp. 511–513, Sep. 2002.

[83] A. Rahman, J. Guo, S. Datta, and M. S. Lundstrom, "Theory of ballistic nanotransistors," *IEEE Trans. Electron Devices*, vol. ED-50, no. 9, pp. 1853–1864, Sep. 2003.

[84] M. S. Lundstrom and J. Guo, *Nanoscale Transistors*. Boston, MA, USA: Springer, 2006.

[85] S. Datta, *Electronic Transport in Mesoscopic Systems*. Cambridge, U.K.: Cambridge Univ. Press, 1997.

[86] M. Lundstrom and Z. Ren, "Essential physics of carrier transport in nanoscale MOSFETs," *IEEE Trans. Electron Devices*, vol. 49, no. 1, pp. 133–141, Jan. 2002.

[87] A. P. Dmitriev and M. S. Shur, "Ballistic admittance: Periodic variation with frequency," *Appl. Phys. Lett*, vol. 89, Oct. 2006, Art. no. 142102. [Online]. Available: http://www.virtualjournals.org/vjs/notification.jsp

[88] K. Natori, H. Iwai, and K. Kakushima, "Anomalous degradation of low-field mobility in short-channel metal-oxide-semiconductor field-effect transistors," *J. Appl. Phys.*, vol. 118, no. 23, Dec. 2015, Art. no. 234502.

[89] M. Lundstrom and C. Jeong, *Near-Equilibrium Transport: Fundamentals and Applications*. Singapore: World Scientific, 2013.

[90] J. Lin, Y. Wu, J. A. del Alamo, and D. A. Antoniadis, "Analysis of resistance and mobility in InGaAs quantum-well MOSFETs from ballistic to diffusive regimes," *IEEE Trans. Electron Devices*, vol. 63, no. 4, pp. 1464–1470, Apr. 2016.

[91] W. Knap *et al.*, "Plasma wave detection of millimeter wave radiation by silicon field effect transistors," *Appl. Phys. Lett*, vol. 85, no. 4, pp. 675–677 26 July.

[92] D. Antoniadis, "On apparent electron mobility in Si nMOSFETs from diffusive to ballistic regime," *IEEE Trans. Electron Devices*, vol. 63, no. 7, pp. 2650–2656, Jul. 2016, doi: 10.1109/TED.2016.2562739.

[93] M. I. Dyakonov and M. S. Shur, "New hydrodynamic phenomena in electronic fluid," in *Proc. 22nd Int. Conf. Phys. Semiconductors*, vol. 1, D. J. Lockwood, Ed. Singapore: World Scientific, 1995, pp. 811–814.

[94] S. Rudin, G. Rupper, and M. Shur, "Ultimate response time of high electron mobility transistors," *J. Appl. Phys.*, vol. 117, no. 17, May 2015, Art. no. 174502, doi: 10.1063/1.4919706.

[95] M. Shur, A. Muraviev, G. Rupper, and S. Rudin, "THz pulse detection by photoconductive plasmonic high electron mobility transistor with enhanced sensitivity," in *Proc. Device Res. Conf. (DRC)*, 2016, pp. 1–2.

[96] Y. Zhang and M. Shur, "P-diamond, Si, GaN and InGaAs teraFETs," 2020, *arXiv:2006.08460*. [Online]. Available: https://arxiv.org/abs/2006.08460

[97] W. Knap *et al.*, "Nonresonant detection of terahertz radiation in field effect transistors," *J. Appl. Phys.*, vol. 91, no. 11, pp. 9346–9353, Jun. 2002.

[98] M. Shur, "Plasmonic detectors and sources for THz communication and sensing," *Proc. SPIE*, vol. 10639, Dec. 2018, Art. no. 1063929.

[99] X. Liu, T. Ytterdal, V. Yu. Kachorovskii, and M. S. Shur, "Compact terahertz SPICE/ADS model," *IEEE Trans. Electron Devices*, vol. 66, no. 6, pp. 2496–2501, Jun. 2019, doi: 10.1109/TED.2019.2911485.

[100] M. Dyakonov and M. S. Shur, "Shallow water analogy for a ballistic field effect transistor: New mechanism of plasma wave generation by dc current," *Phys. Rev. Lett.*, vol. 71, no. 15, pp. 2465–2468, Oct. 1993.

[101] V. Ryzhii, "Plasma instability and terahertz generation in HEMTs due to electron transit-time effect," *IEICE Trans. Electron.*, vols. E89–C, no. 7, pp. 1012–1019, Jul. 2006.

[102] W. Knap *et al.*, "Emission of terahertz radiation by plasma waves in 60 nm AlInAs/InGaAs high electron mobility transistors," *Appl. Phys. Lett.*, vol. 84, no. 13, pp. 2331–2333, Mar. 2004.

[103] J. Lusakowski *et al.*, "Voltage tuneable terahertz emission from a ballistic nanometer InGaAs-InAlAs transistor," *J. Appl. Phys.*, vol. 97, no. 6, Mar. 2005, Art. no. 064307.

[104] S. Boubanga-Tombet *et al.*, "Current driven resonant plasma wave detection of terahertz radiation: Toward the Dyakonov–Shur instability," *Appl. Phys. Lett.*, vol. 92, no. 21, May 2008, Art. no. 212101.

[105] T. Watanabe, A. Satou, T. Suemitsu, W. V. V. Knap Popov, and T. Otsuji, "Plasmonic terahertz monochromatic coherent emission from an asymmetric chirped dual-grating-gate InP-HEMT with a photonic vertical cavities," in *Proc. CLEO, Conf. Lasers Electrooptics Dig.*, San Jose, CA, USA, Jun. 2013, pp. 1–9.

[106] E. Dyakonova, A. El Fatimy, and J. Sakowski, "Room-temperature terahertz emission from nanometer field-effect transistors," *Appl. Phys. Lett.* vol. 88, no. 14, 2006, Art. no. 141906.

[107] Y. Zhou, X. Li, and R. Tan, "Extraction of terahertz emission from a grating-coupled high-electron-mobility transistor," *J. Semicond.*, vol. 34, no. 2, 2013, Art. no. 022002.

[108] Y. M. Meziani *et al.*, "Room temperature terahertz emission from grating coupled two-dimensional plasmons," *Appl. Phys. Lett.*, vol. 92, no. 20, May 2008, Art. no. 201108.

[109] T. Onishi, T. Tanigawa, and S. Takigawa, "High power terahertz emission from a single gate AlGaN/GaN field effect transistor with periodic ohmic contacts for plasmon coupling," *Appl. Phys. Lett.*, vol. 97, no. 9, Aug. 2010, Art. no. 092117.

[110] S. Kim, S. Hong, and J. Jang, "Strong and narrowband terahertz radiation from GaAs based pHEMT and terahertz imaging," *Microw. Opt. Technol. Lett.*, Jul. 2020.

[111] M. Dyakonov and M. Shur, "Detection, mixing, and frequency multiplication of terahertz radiation by two-dimensional electronic fluid," *IEEE Trans. Electron Devices*, vol. 43, no. 3, pp. 380–387, Mar. 1996.

[112] M. I. Dyakonov and M. S. Shur, "Plasma wave electronics: Novel terahertz devices using two-dimensional electron fluid, special issue on future directions in device science and technologies," *IEEE Trans. Electron Devices*, vol. 43, no. 10, pp. 1640–1646, Oct. 1996.

[113] X. Liu, T. Ytterdal, and M. Shur, "Plasmonic FET terahertz spectrometer," *IEEE Access*, vol. 24, pp. 56039–56044, 2020.

[114] M. S. Shur, *Introduction to Electronic Devices*. Hoboken, NJ, USA: Wiley, 1996.

[115] G. R. Aizin, J. Mikalopas, and M. Shur, "Plasmonic instabilities in two-dimensional electron channels of variable width," *Phys. Rev. B, Condens. Matter*, vol. 101, no. 24, Jun. 2020, Art. no. 245404.

[116] W. Stillman *et al.*, "Nanometer scale complementary silicon MOSFETs as detectors of terahertz and sub-terahertz radiation," in *Proc. IEEE Sensors*, 2007, pp. 479–480.

[117] W. Stillman *et al.*, "Silicon FIN FETs as detectors of terahertz and sub-terahertz radiation," *Int. J. High Speed Electron. Syst.*, vol. 20, no. 1, pp. 27–42, Mar. 2011.

[118] M. Shur, S. Rudin, G. Rupper, and T. Ivanov, "P-diamond as candidate for plasmonic terahertz and far infrared applications," *Appl. Phys. Lett.*, vol. 113, no. 25, Dec. 2018, Art. no. 253502, doi: 10.1063/1.5053091.

[119] V. Ryzhii, T. Otsuji, and M. Shur, "Graphene plasmonics for terahertz applications," *Appl. Phys. Lett.*, vol. 116, Art. no. 140501, May 2020.

[120] I. V. Gorbenko, V. Y. Kachorovskii, and M. Shur, "Terahertz plasmonic detector controlled by phase asymmetry," *Opt. Express*, vol. 27, no. 4, pp. 4004–4013, Feb. 2019, doi: 10.1364/OE.27.004004.

[121] J. Park, X. Liu, T. Ytterdal, and M. Shur, "Carbon nanotube detectors and spectrometers for the terahertz range," *Crystals*, vol. 10, no. 7, p. 601, Jul. 2020, doi: 10.3390/cryst10070601.

[122] A. Lisauskas, U. Pfeiffer, E. Öjefors, P. H. Bolìvar, D. Glaab, and H. G. Roskos, "Rational design of high-responsivity detectors of terahertz radiation based on distributed self-mixing in silicon field-effect transistors," *J. Appl. Phys.*, vol. 105, Dec. 2009, Art. no. 114511.

[123] E. L. Ivchenko and S. D. Ganichev, "Ratchet effects in quantum wells with a lateral superlattice," *JETP Lett.*, vol. 93, no. 11, pp. 673–682, Aug. 2011, doi: 10.1134/S002136401111004X.

[124] G. Rupper, S. Rudin, and M. Shur, "Ratchet effect in AlGaAs/InGaAs multi-finger high electron mobility transistors," in *Proc. Compound Semiconductor Week*, 2018, pp. 279–280.
[125] G. Rupper, S. Rudin, and M. S. Shur, "Ratchet effect in partially gated multifinger field-effect transistors," *Phys. Rev. A, Gen. Phys.*, vol. 9, no. 6, Jun. 2018, Art. no. 064007.
[126] P. Olbrich *et al.*, "Ratchet effects induced by terahertz radiation in heterostructures with a later al periodic potential," *PRL*, vol. 103, May 2009, Art. no. 090603.
[127] P. Olbrich *et al.*, "Classical ratchet effects in heterostructures with a lateral periodic potential," *Phys. Rev. B, Condens. Matter*, vol. 83, no. 16, Apr. 2011, Art. no. 165320.
[128] I. V. Rozhansky, V. Y. Kachorovskii, and M. S. Shur, "Helicity-driven ratchet effect enhanced by plasmons," *Phys. Rev. Lett.*, vol. 114, no. 24, Jun. 2015, Art. no. 246601.
[129] T. Watanabe *et al.*, "Plasmonic terahertz monochromatic coherent emission from an asymmetric chirped dual-grating-gate InP-HEMT with highly asymmetric resonant cavities," *The 3rd Russia-Japan-USA Symp., Jun. 17-21, Book Abstr.*, pp. 39–40 (2014).
[130] V. V. Popov, D. V. Fateev, O. V. Polischuk, and M. S. Shur, "Enhanced electromagnetic coupling between terahertz radiation and plasmons in a grating-gate transistor structure on membrane substrate," *Opt. Express*, vol. 18, no. 16, p. 16771, Aug. 2010.
[131] A. V. Muravjov *et al.*, "Temperature dependence of plasmonic terahertz absorption in grating-gate GaN HEMT structures," *Appl. Phys. Lett*, vol. 96, May 2010, Art. no. 042105.
[132] D. V. Lavrukhin *et al.*, "Terahertz photoconductive emitter with dielectric-embedded high-aspect-ratio plasmonic grating for operation with low-power optical pumps," *AIP Adv.*, vol. 9, no. 1, Jan. 2019, Art. no. 015112, doi: 10.1063/1.5081119.
[133] M. Karabiyik *et al.*, "Plasmonic properties of asymmetric dual grating gate plasmonic crystals," *Phys. Status Solidi*, vol. 253, no. 4, pp. 671–675, Apr. 2016, doi: 10.1002/pssb.201552609.
[134] V. Y. Kachorovskii and M. S. Shur, "Current-induced terahertz oscillations in plasmonic crystal," *Appl. Phys. Lett.*, vol. 100, no. 23, Jun. 2012, Art. no. 232108.
[135] G. R. Aizin, J. Mikalopas, and M. Shur, "Current driven 'plasmonic boom' instability gated periodic ballistic nanostructures," *Phys. Rev. B, Condens. Matter*, vol. 93, no. 19, May 2016, Art. no. 195315.
[136] X. Peralta *et al.*, "THz detection by resonant 2-D plasmons in field effect devices," *Int. J. High Speed Electron. Systems.*, vol. 12, no. 3, pp. 925–937 2002.
[137] G. C. Dyer *et al.*, "Enhanced performance of resonant sub-terahertz detection in a plasmonic cavity," *Appl. Phys. Lett.*, vol. 100, no. 8, Feb. 2012, Art. no. 083506.
[138] N. Pala, D. Veksler, A. Muravjov, W. Stillman, R. Gaska, and M. S. Shur, "Resonant detection and modulation of terahertz radiation by 2DEG plasmons in GaN grating-gate structures," in *Proc. IEEE Sensors*, Oct. 2007, pp. 291–292.
[139] G. C. Dyer, G. R. Aizin, J. L. Reno, E. A. Shaner, and S. J. Allen, "Novel tunable millimeter-wave grating-gated plasmonic detectors," *IEEE J. Sel. Topics Quantum Electron.*, vol. 17, no. 1, pp. 85–91, Jan. 2011.
[140] T. A. Elkhatib *et al.*, "Enhanced plasma wave detection of terahertz radiation using multiple high electron-mobility transistors connected in series," *IEEE Trans. Microw. Theory Techn.*, vol. 58, no. 2, pp. 331–339, Feb. 2010.
[141] V. V. Popov *et al.*, "High-responsivity terahertz detection by on-chip InGaAs/GaAs field-effect-transistor array," *Appl. Phys. Lett.*, vol. 98, no. 15, Apr. 2011, Art. no. 153504.
[142] G. R. Aizin, V. V. Popov, and O. V. Polischuk, "Plasmon enhanced electron drag and terahertz photoconductance in a grating-gated field-effect transistor with two-dimensional electron channel," *Appl. Phys. Lett.*, vol. 89, no. 14, Oct. 2006, Art. no. 143512.
[143] V. V. Popov, G. M. Tsymbalov, D. V. Fateev, and M. S. Shur, "Cooperative absorption of terahertz radiation by plasmon modes in an array of field-effect transistors with two-dimensional electron channel," *Appl. Phys. Lett.*, vol. 89, no. 12, Sep. 2006, Art. no. 123504.
[144] G. R. Aizin, D. V. Fateev, G. M. Tsymbalov, and V. V. Popov, "Terahertz plasmon photoresponse in a density modulated two-dimensional electron channel of a GaAs-AlGaAs field-effect transistor," *Appl. Phys. Lett.*, vol. 91, no. 16, Oct. 2007, Art. no. 163507.
[145] T. V. Teperik, F. J. García de Abajo, V. V. Popov, and M. S. Shur, "Strong terahertz absorption bands in a scaled plasmonic crystal," *Appl. Phys. Lett.*, vol. 90, no. 25, Jun. 2007, Art. no. 251910.
[146] A. S. Petrov, D. Svintsov, V. Ryzhii, and M. S. Shur, "Amplified-reflection plasmon instabilities in grating-gate plasmonic crystals," *Phys. Rev. B, Condens. Matter*, vol. 95, no. 4, Jan. 2017, Art. no. 045405.
[147] G. R. Aizin, J. Mikalopas, and M. Shur, "Current-driven dyakonov-shur instability in ballistic nanostructures with a stub," *Phys. Rev. A, Gen. Phys.*, vol. 10, no. 6, Dec. 2018, Art. no. 064018, doi: 10.1103/PhysRevApplied.10.064018.

Michael S. Shur (Life Fellow, IEEE) received the M.S. degree in electrical engineering from St. Petersburg Electrotechnical University, and the Ph.D. degree in mathematics and physics and the D.Sc. (Habilitation) degree in mathematics and physics from the A. F. Ioffe Institute of Physics and Technology. He is currently the Patricia W. and Patricia W. and C. Sheldon Roberts Professor of Solid State Electronics and a Professor of Physics, Applied Physics, and Astronomy with the Rensselaer Polytechnic Institute, Troy, NY, USA. He is a Life Fellow of the American Physical Society and SPIE, and a Fellow of OSA, SPIE, IET, AAAS, MRS, WIF, and ECS. He is also a Foreign Member of Lithuanian Academy of Sciences and a Fellow of the National Academy of Inventors. His awards include the Tibbetts Award for Technology Commercialization, the Honorary Doctorates from the St. Petersburg Technical University and University of Vilnius, the IEEE EDS Ebers Award, the Sensors Council Technical Achievement Award, the IEEE Donald Fink Award, the IEEE Kirchmayer Award, the Gold Medal of the Russian Ministry of Education, the van der Ziel Award, the Senior Humboldt Research Award, the Pioneer Award, the RPI Engineering Research Award, several best paper awards, and Distinguished Lecturer awards from the IEEE EDS, MTT, and Sensors Council. He is also the Editor-in-Chief of the *International Journal of High Speed Electronics and Systems*.